In Situ and *Ex Situ* TEM Analysis of the Copper Precipitation in Martensitic Steel

MARGARITA D. BAMBACH, ŁUKASZ SZCZEPAŃSKI, and ANDRZEJ M. ŻAK

The conventional and *in situ* transmission electron microscopy imaging of quenched 1.5 pct Cu steel has shown that Cu phases are present even before aging and do not disappear after typical aging times. The 9R precipitates appear after 15 minutes of heating, but they are more noticeable after longer processing times. This suggests that the precipitation mechanisms in carbon steels deserve further analysis, especially because of the inevitable increase in the Cu content in the steel ingots.

https://doi.org/10.1007/s11661-021-06561-6

THE volume of copper in end-of-life steel scrap is constantly increasing.[1] The problem of reducing the amount of Cu in recycled steel remains an unresolved issue,[2] prompting the search for new solutions for alloy purification.[3,4] Despite this, the unintentional content of this impurity already regularly reaches 0.3 pct and could even exceed 0.5 pct.[5] This fact raises the following problems: (i) the Cu content can easily exceed the value of 0.4 pct, already classified as an alloying value; (ii) once it has entered the steel circulation cycle, it is very difficult to remove copper through conventional metallurgy; (iii) separating the copper-free steel scrap from the copper-contaminated one leads to an increased logistic effort.[1] At the same time, steel recycling is essential to preserve resources and meet global challenges. Instead of focusing on the metallurgical means to increase the purity of recycled steel, copper could be used to trigger strength increase mechanisms if the yield strength of the material has been reached locally during component service. Thus, it can prevent preliminary failure and increase the component's life. The concept of this damage tolerance approach for copper-alloyed gear steels has been described in previous work by one of the authors.[6] It was shown that such copper-alloyed steels possess an increased strain-hardening behavior as well as damage tolerance under both static and cyclic loading. Cu content also affects the corrosion and tribological properties of bearing steels.[7] However, to obtain the expected mechanical parameters and microstructure of Cu-contaminated steel, a profound understanding of the kinetics of formation and transformation of the nanosized copper precipitates is necessary.

The question of analyzing the kinetics of strengthening of the Fe-Cu alloy by quenching and aging has been analyzed intensively for over a half century.[8] The amount of Cu in the steels tested in the last decade ranged from 1.15 pct,[9] through 1.53 pct,[10] up to more popular, higher values reaching 2.00 pct,[11,12] 2.12 pct,[13,14] 2.50 pct,[15,16] and even 5.50 pct.[17] The analyzed materials were mainly low carbon, containing less than 0.1 pct.,[13] less than 0.05 pct.,[9,18] or even less than 0.01 pct.[11,12,16] Only articles[10] and[19] referred to alloys with a carbon content of 0.44 pct and 0.27 pct, respectively.

It is well known that quenching from the austenite region and tempering at around 673 K to 923 K[18] of Cu-alloyed steels leads to the formation of nanosized copper precipitates that increase the strength of low-C ferritic steels. The nucleation and growth of copper-rich precipitates are still a subject of debate and development. The most established model of Cu precipitates growth includes coherent BCC Cu zones, undergoing the martensitic transformation to semi-coherent 9R phase, through 3R particles into incoherent FCC ε-Cu.[9,12] The development of the structure is also variable from the content of other alloying elements, making the unambiguous classification of nucleation difficult.[13] The lattice parameters of the subsequent possible phases are summarized in Table I.

It has been reported recently that precipitates may be present as nano-Fe-Cu-ordered clusters with an ordered B2 structure at the initial stage of their formation.[13,14,16] However, in the case of martensitic steels,

MARGARITA D. BAMBACH is with the Gesellschaft für metallurgische Software- und Technologieentwicklung (GMT) mbH, Börnicker Chaussee 1-2, 16321 Bernau, Germany. ŁUKASZ SZCZEPAŃSKI and ANDRZEJ M. ŻAK are with the Faculty of Mechanical Engineering, Wroclaw University of Science and Technology (WUST), Wybrzeze Wyspianskiego 27, 50370 Wroclaw, Poland. Contact e-mail: andrzej.zak@pwr.edu.pl
Manuscript submitted August 25, 2021; accepted November 25, 2021. Article published online January 25, 2022

Table I. Probable Phases in Supersaturated and Aged Fe-Cu Steel

Phase	Lattice Type	Crystallographic Parameters	Size	Source
α—Fe	cubic FCC	$a = 0.2866$ nm, $\alpha = 90$ deg	matrix	—
BCC—Cu	cubic BCC	$a = 0.2887$ nm, $\alpha = 90$ deg	2 to 4 nm	13
9R—Cu	orthorhombic	$a = 0.4330$ nm, $b = 0.2500$ nm $c = 1.836$ nm $\alpha = 90$ deg, $\beta = 86$ deg, $\gamma = 90$ deg	8 to 20 nm	20
FCC—Cu	cubic FCC	$a = 0.3615$ nm, $\alpha = 90$ deg	50 to 100 nm	21

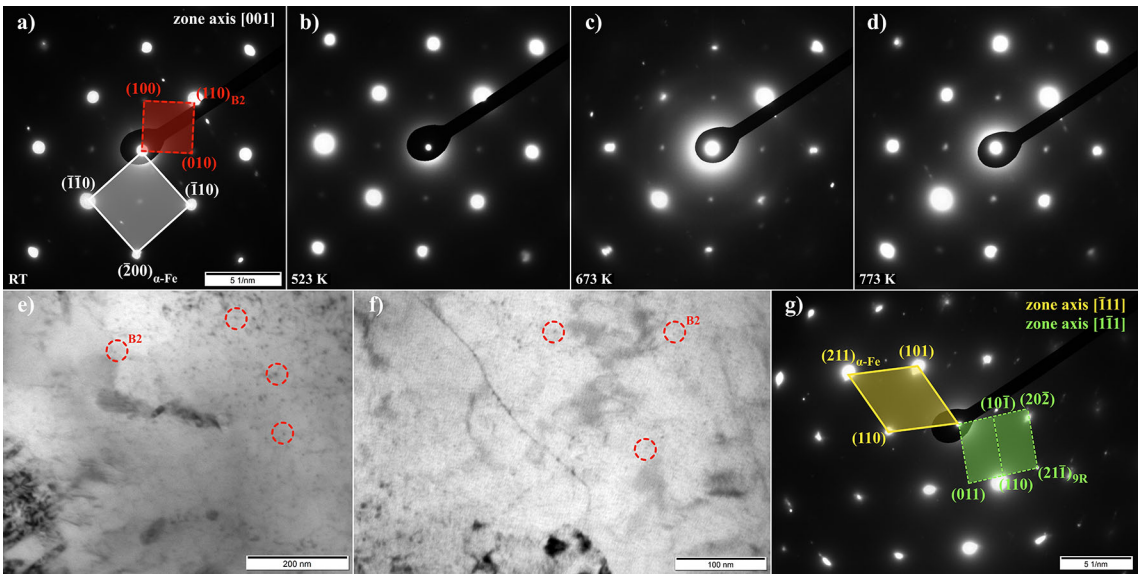

Fig. 1—Bright-field images (*e, f*) and SAED patterns (*a, b, c, d, g*) taken in the [001] zone axis at room temperature (a, e, g), during *in situ* TEM heating at 523 K (b), 673 K (c), and 773 K (d), and after post-heating ion cleaning (f, g).

the increase in hardness during Cu precipitation counteracts material softening during tempering.[6,22] Here, trivial tempering curves cannot be used to determine the peak strength since the material softening dominates over the strength increase due to aging. Most of the analyses on Cu precipitation concern only low-carbon steel. However, an increase in carbon content has been reported to delay Cu precipitation by decreasing the diffusion coefficient of Cu, whereas temperature has a much stronger effect on Cu diffusion in Fe.[22,23] Cementite interfaces serve as nucleation sites for fcc-Cu precipitates, whereas bcc-Cu is formed in the material matrix. The strength increase, however, has been assigned to the increased volume fraction of M_2C particles following the Cu precipitation.[10,24] Last but not least, Cu precipitation in martensitic steels has been reported to increase both the static and cyclic strain-hardening exponent during mechanical loading.[10]

Since conventional tempering curves cannot yield the necessary information on the critical particle size and the peak strength in martensitic steels, it is of tremendous importance to understand the kinetics of Cu precipitate formation and transformation so that suitable aging parameters can be chosen to adjust an optimum particle size both in accidentally contaminated and intentionally alloyed steel. Once the precipitation sequence for the given composition is revealed, the optimal heat treatment parameters can be set. Then, microstructure engineering can be used to tailor the local material properties by adjusting a material matrix for increased damage tolerance.

For this purpose, parallel *ex situ* and *in situ* transmission electron microscopy (TEM) analyses have been utilized to reveal the precipitation sequence as well as to study the orientation relationship between the nanosized copper precipitates and the martensitic matrix in a copper-alloyed martensitic steel grade with increased carbon content for gearbox applications. The copper content was set to visualize the studied phenomena more clearly, and at the same time to keep the Cu content within the limits that were not significantly different from the standard accidental contamination.

A standard martensitic 0,18C-1,5Cr-1,5Ni-0,3Mo steel has been alloyed with 1.5 mass pct Cu. More information about the chemical composition and metallurgical processing of steel is available in previous work.[6] The blanks have been treated by solution annealing at 1123 K for 10 minutes followed by oil quenching to room temperature. Samples in this state

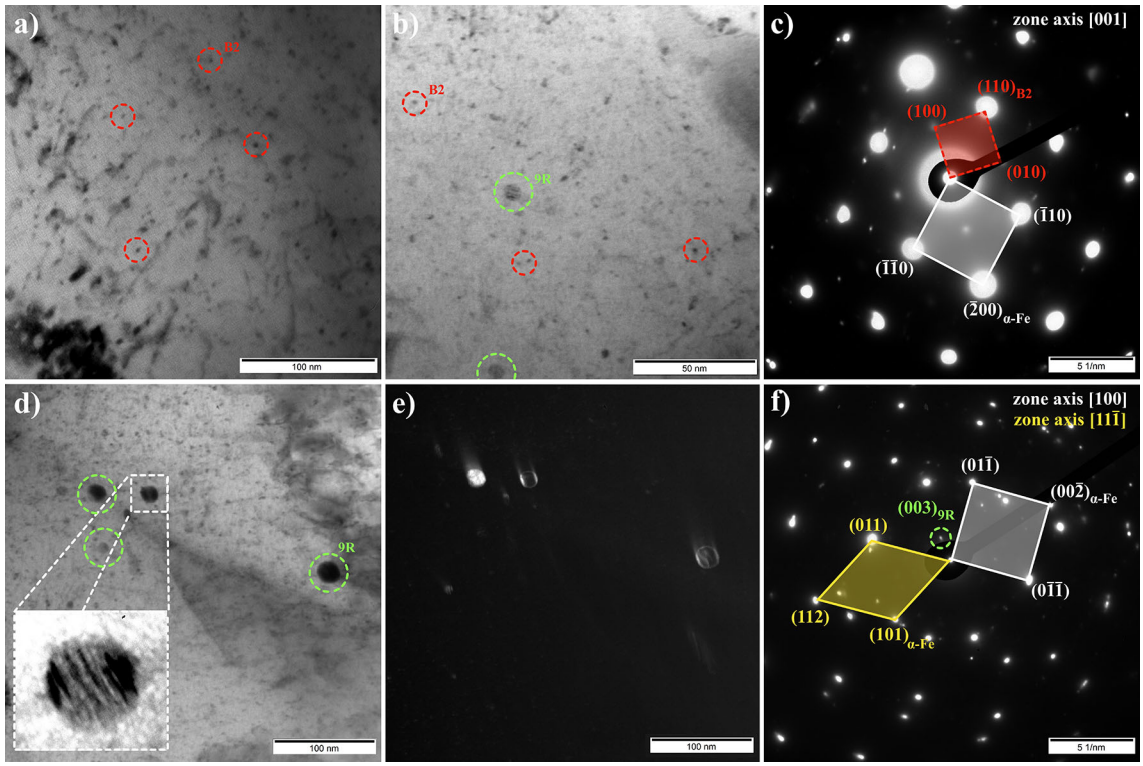

Fig. 2—Bright-field (*a, b, d*), dark-field images (*e*), and SAED patterns (*c, f*) taken from *ex situ* samples aged for 166 minutes at 773 K.

were the basis for testing as-quenched and *in situ* annealed samples. An additional sample was furnace aged at 773 K for 166 min. The aging condition was defined as 'peak strength' and was determined in previous studies.[6]

The samples for TEM observations were prepared using mechanical thinning to a thickness of 100 μm and cutting to 3mm disks (Disc Punch, Gatan), followed by electrolytic polishing (TenuPol, Struers) and then ion polishing (DuoMill, Gatan) for 2 minutes to remove contamination and polishing products. The samples were observed using a Hitachi H-800 TEM. The microscope was equipped with a modified Hitachi heating holder. For the *in situ* tests, the heating rate was approximately 10 K/min to heat the sample from room temperature to 773 K. The selected area electron diffraction (SAED) analyses were performed with the open-source software CrysTBox.[25,26] To ensure that ordered structures such as B2 are made visible, the [001] and [110] zone axes have been used for observation among other orientations. Some of the biggest challenges related to the TEM analysis of Cu precipitates in martensite are the low coherence strain between precipitates and matrix and the reduced observation time due to sample contamination. After *in situ* annealing for 15 K minutes at 773 K and observations, the sample was cooled and cleaned from observation-related contamination with ion polishing methods for 30 seconds, and additional characterization at normal conditions was performed.

The structure in as-quenched condition revealed typical martensitic grains with a significant amount of nucleated precipitates (Figure 1(e)). The electron diffraction pattern allows identifying the precipitations as BCC-B2 particles (Figure 1(a)). In general, the {100} diffraction spots at the zone axis [001] in pure α-Fe iron are not visible because the scattering amplitude of Fe atoms to electrons is the same, and therefore, the intensity of the scattered wave is equal to zero. In the case of a B2 structure, however, Cu and Fe have different scattering amplitudes to electrons, leading to the appearance of diffraction spots in the forbidden reflection area, confirming the presence of an ordered nanostructure.[14] According to the literature,[12–14] it is considered that these ordered B2 nanostructures are Fe-Cu precipitates, characterized by the substitution arrangement of copper atoms in the alpha iron (α-Fe) cell. Moreover, the measured average size of the B2 precipitates of 2 to 5 nm fits well to the literature values.[13,14] Increasing the temperature during the *in situ* heating resulted in changing only the intensity of the superlattice diffraction spots indicating growth of the B2 precipitates (Figures 1(b) through (d)). Diffraction spots from the 9R Cu structure were not detected during direct *in situ* imaging. The formation of a thin contamination layer covering the sample could be a possible reason for the difficulty to detect 9R Cu precipitates within the sample. At the same time, the bright-field imaging revealed not only the presence of B2 dispersed precipitates but also the tweed pattern (Figure 1(f)). In addition, further ion cleaning revealed the presence of precipitates that can be recognized as 9R

(Figure 1(g)). However, after 15 minutes *in situ* heat treatment, their volume fraction is still significantly lower than the one of the B2 precipitates.

It is possible that the heating rate was too high and the aging time too short to allow phase transformation into the 9R structure, suggesting significant stability of the B2 phase and slow transformation kinetics. Due to the small volume fraction of precipitated particles (1.16 vol. pct calculated from SANS measurements[6]) and the relatively low Cu content of the alloy related to the long diffusion ways of the copper atoms within the matrix, the diffusion-based growth of B2 particles is prolonged. Moreover, the diffusion coefficient of copper atoms could be decreased by the increase in C content as described in the literature.[22,23] As a result, B2 precipitates do not reach the critical size associated with the transformation to the 9R structure and remain longer stable. This assumption is supported by the fact that a large volume fraction of B2 precipitates was detected after 166 minutes of aging at 773 K. The *ex situ* treated sample allows us to recognize similar homogeneously distributed B2 particles both on bright-field images (Figures 2(a) and (b)) and on SAED patterns (Figure 2(c)). Additionally, small amounts of 9R precipitates with a size of 8 to 20 nm were observed (Figures 2(b) and (d)). The typical "coffee-bean" structures as observed by *e.g.*,[27] which are characteristic for the semi-coherent 9R Cu precipitates could be visualized by dark-field TEM (Figure 2(e)) taken from the 003_{9R} spot in the SAED pattern (Figure 2(f)). The latter, however, shows only one spot corresponding to the interplanar distance of the 9R plane (003). Dark-field observation excluded the possibility that the single point might be the effect of double diffraction or forbidden reflection of the matrix.

In both the *in situ* as well as the *ex situ* treated samples, there were a large volume fraction of the ordered B2 structures and the tweed pattern of the matrix detected. The B2 particles were detectable even in the as-quenched sample, which means that they evolved naturally during cooling or natural aging under storage. The low activation energy of Cu precipitate formation associated with an increased C content of the alloy and cementite formation prior to copper precipitation has already been reported by Jung.[10] Consequently, copper phases have a significant effect on the increase in strength and hardening of Cu-alloyed steel, as determined in previous research.[6] *In situ* TEM revealed that further B2 precipitation begins immediately after the heating begins. The B2 to 9R transformation started in the first 15 minutes of aging, but a significant amount of this phase was visible after longer heating for 166 min. The slow transformation kinetics here are also related to the delayed growth of the B2 precipitates, as explained above. For the investigated alloy, the B2-9R transformation could be observed in the tested temperature and time range, but the optimal aging time should be determined depending on the application, based on mechanical tests.[6] To be able to quantify the effect of the C content on the kinetics of transformation in the Fe-C-Cu system, further work is required.

Based on the results shown above, it can be concluded that

- B2-structured precipitates could be identified in both the as-quenched, *in situ*, and *ex situ* aged sample. These are most probably nanosized ordered Fe-Cu precipitates, partially coherent with the martensitic matrix. The B2 phases remain stable at prolonged heating times (166 minutes at 773 K).
- *In situ* TEM showed the development of B2 structures and tweed patterns in the matrix immediately after the onset of heating. The insignificant amount of 9R phases could be observed *in situ* even after 15 minutes of heating up to 773 K, but only a longer *ex situ* treatment allows easy observation of such precipitates. This means that aging time is as important processing variable as temperature, even in the unrepresentative 2D thin-film volume used in *in situ* TEM studies.

Dr. Ing. Margarita D. Bambach acknowledges funding received from the Brandenburg Technical University Cottbus-Senftenberg for staying at the Wrocław University of Science and Technology in Poland to conduct the TEM analysis. The authors thank Prof. Dr. Ing. Włodzimierz Dudziński for the discussions.

Margarita Bambach is an employee of the *Gesellschaft für Metallurgische Software- und Technologieentwicklung (GMT) mbH*, but this publication is not related to her employment. Because of that, on behalf of all authors, the corresponding authors state that there is no conflict of interest.

OPEN ACCESS

REFERENCES

1. K.E. Daehn, A. Cabrera Serrenho, and J.M. Allwood: *Environ. Sci. Technol.*, 2017, vol. 51, pp. 6599–6606.
2. K.E. Daehn, A.C. Serrenho, and J. Allwood: *Metall and Materi Trans B.*, 2019, vol. 50, pp. 1225–40.

3. Z. Lu and C. Liu: *ISIJ Int*., 2020, vol. 60, pp. 2625–7.
4. Z. Lu, C. Liu, and Y. Wang: *J. Electrochem. Soc*., 2021, vol. 168, p. 36508.
5. I. Daigo, K. Tajima, H. Hayashi, D. Panasiuk, K. Takeyama, H. Ono, Y. Kobayashi, K. Nakajima, and T. Hoshino: *ISIJ Int*., 2021, vol. 61, pp. 498–505.
6. M.D. Bambach, W. Bleck, H.S. Kramer, M. Klein, D. Eifler, T. Beck, H. Surm, H.-W. Zoch, F. Hoffmann, and A. Radulescu: *Steel Res. Int*., 2016, vol. 87, pp. 550–61.
7. S. Yeşiltepe and M.K. Şeşen: *SN Appl. Sci*., 2020, vol. 2, p. 149.
8. A. Youle and B. Ralph: *Metal Sci. J*., 1972, vol. 6, pp. 149–52.
9. L. Han, Q. Liu, and J. Gu: *Chin. J. Mech. Eng*., 2019, https://doi.org/10.1186/s10033-019-0397-8.
10. J.-G. Jung, M. Jung, S.-M. Lee, E. Shin, H.-C. Shin, and Y.-K. Lee: *J. Alloy. Compd*., 2013, vol. 553, pp. 299–307.
11. M. Sun, W. Zhang, Z. Liu, and G. Wang: *Mater. Lett*., 2017, vol. 187, pp. 49–52.
12. Y.-U. Heo, Y.-K. Kim, J.-S. Kim, and J.-K. Kim: *Acta Mater*., 2013, vol. 61, pp. 519–28.
13. G. Han, Z.J. Xie, B. Lei, W.Q. Liu, H.H. Zhu, Y. Yan, R. Misra, and C.J. Shang: *Mater. Sci. Eng. A*., 2018, vol. 730, pp. 119–36.
14. G. Han, Z.J. Xie, Z.Y. Li, B. Lei, C.J. Shang, and R. Misra: *Mater. Des*., 2017, vol. 135, pp. 92–101.
15. Y.R. Wen, A. Hirata, Z.W. Zhang, T. Fujita, C.T. Liu, J.H. Jiang, and M.W. Chen: *Acta Mater*., 2013, vol. 61, pp. 2133–47.
16. Y.R. Wen, Y.P. Li, A. Hirata, Y. Zhang, T. Fujita, T. Furuhara, C.T. Liu, A. Chiba, and M.W. Chen: *Acta Mater*., 2013, vol. 61, pp. 7726–40.
17. V.N. Urtsev, D.A. Mirzaev, I.L. Yakovleva, N.A. Tereshchenko, and K.Y. Okishev: *Phys. Metals Metall*., 2010, vol. 110, pp. 346–55.
18. A. Deschamps, M. Militzer, and W.J. Poole: *ISIJ Int*., 2001, vol. 41, pp. 196–205.
19. D. Isheim, M.S. Gagliano, M.E. Fine, and D.N. Seidman: *Acta Mater*., 2006, vol. 54, pp. 841–9.
20. T.-H. Lee, Y.-O. Kim, and S.-J. Kim: *Phil. Mag*., 2007, vol. 87, pp. 209–24.
21. R. Monzen, M. Iguchi, and M.L. Jenkins: *Philos. Mag. Lett*., 2000, vol. 80, pp. 137–48.
22. N. Maruyama, M. Sugiyama, T. Hara, and H. Temehiro: *Mater. Trans*., 1999, vol. 40, pp. 268–77.
23. M. El-Sayed and A. Rassoul: *J. Mater. Sci*., 1997, vol. 32, pp. 6471–4.
24. B.L. Tiemens, A.K. Sachdev, and G.B. Olson: *Metall. Mater. Trans. A*., 2012, vol. 43, pp. 3615–25.
25. M. Klinger: *CrysTBox—Crystallographic Toolbox*, Institute of Physics of the Czech Academy of Sciences, Prague, 2015.
26. M. Klinger and A. Jäger: *J. Appl. Crystallogr*., 2015, vol. 48, pp. 2012–8.
27. P.J. Othen, M.L. Jenkins, and G.D.W. Smith: *Philos. Mag. A*., 1994, vol. 70, pp. 1–24.